Accepted Manuscript

The effect of pore-former morphology on the electrochemical performance of solid oxide fuel cells under combined fuel cell and electrolysis modes

Miguel A. Laguna-Bercero, Amir R. Hanifi, Lucile Menand, Navjot K. Sandhu, Neil E. Anderson, Thomas H. Etsell, Partha Sarkar

PII: S0013-4686(18)30337-2

DOI: 10.1016/j.electacta.2018.02.055

Reference: EA 31250

To appear in: *Electrochimica Acta*

Received Date: 8 November 2017

Revised Date: 9 February 2018

Accepted Date: 10 February 2018

Please cite this article as: M.A. Laguna-Bercero, A.R. Hanifi, L. Menand, N.K. Sandhu, N.E. Anderson, T.H. Etsell, P. Sarkar, The effect of pore-former morphology on the electrochemical performance of solid oxide fuel cells under combined fuel cell and electrolysis modes, *Electrochimica Acta* (2018), doi: 10.1016/j.electacta.2018.02.055.

The Effect of Pore-former Morphology on the Electrochemical Performance of Solid Oxide Fuel Cells under Combined Fuel Cell and Electrolysis Modes

Miguel A. Laguna-Bercero[1*], Amir R. Hanifi[2], Lucile Menand[3], Navjot K. Sandhu[2], Neil E. Anderson[2], Thomas H. Etsell[2], and Partha Sarkar[4]

[1]Instituto de Ciencia de Materiales de Aragón (ICMA), CSIC- Universidad de Zaragoza, C/ Pedro Cerbuna 12, E-50009, Zaragoza, Spain

[2]Department of Chemical & Materials Engineering, University of Alberta, Edmonton, Alberta T6G 1H9, Canada

[3] Institut Universitaire de Technologie de Bordeaux (IUT), Université Bordeaux, 15 rue Naudet - CS 10207, 33 175 Gradignan Cedex, France

[4]InnoTech Alberta, Edmonton, Alberta. T6N 1E4, Canada

*Corresponding author's e-mail: malaguna@unizar.es

Abstract

The effect of the pore-former used in the Ni-YSZ fuel electrode on the electrochemical performance of solid oxide cells is studied. Three cells with the configuration of Ni-YSZ/YSZ/$Nd_2NiO_{4+\delta}$-YSZ were fabricated with different pore-formers, such as graphite, PMMA (polymethyl methacrylate) or an equal mixture of both, which were added to the Ni-YSZ support during the fabrication process. The results show that the Ni-YSZ support containing graphite leads to a more porous support and formation of coarser pores in the vicinity of the electrolyte. This leads to a reduction in the triple phase boundary (TPB) length with a corresponding increase of activation polarization and, as a consequence, the overall cell performance decreases in both

fuel cell and electrolysis modes. The cell having PMMA delivered the highest performance under both operation modes (818 and -713 $mAcm^{-2}$ were obtained in SOFC and SOEC modes at 800 ºC), due to finer pores next to the electrolyte. The cell having the mixture of both pore-formers delivered intermediate results. All the cells show similar concentration polarization values meaning that even the least porous cell (PMMA) provided sufficient porosity for gas flow. In addition, long term reversible experiments were performed, showing no degradation for a period above 400 hours.

Keywords: Tubular; Nickel; Zirconia; Microstructure; Pore-former; SOFC; SOEC

Introduction

Solid oxide fuel cell (SOFC) technology is a clean and efficient method of electricity production which functions through electrochemical oxidation of a fuel such as hydrogen at high temperatures. A solid oxide electrolysis cell (SOEC) is a reversible SOFC which produces hydrogen by splitting water molecules when voltage is applied [1,2].

Nickel-YSZ (yttria stabilized zirconia) is the commonly used anode under SOFC and cathode under SOEC modes. In this cermet, nickel provides the electrical conduction path for the released electrons and also acts as a catalyst for oxidation of hydrogen. YSZ is not only the electrolyte for oxygen ion conduction but also forms a porous matrix which provides the required mechanical properties for cell operation at high temperatures, suppresses nickel sintering and reduces the mismatch of the thermal expansion coefficient between the anode and electrolyte [3,4]. Nickel, YSZ and pores together form the triple phase boundaries (TPBs) where they meet in the vicinity of the electrolyte. Electrochemical reactions occur in such locations and electrons are released.

It is known that the gas permeability, electrical conductivity and the rate of reaction in both SOFC and SOEC modes are highly dependent on the Ni-YSZ microstructure including the grain size of the nickel and YSZ phases, porosity and the percolation of each phase [5,6]. For example, it was shown by Han et al. that decreasing the grain size of nickel led to an increased TPB length [7]. Mogensen et al. have also shown that finer YSZ grains led to improved TPB length and fuel cell performance [8]. In addition, the influence of the reducing conditions on Ni-YSZ cermets also plays a crucial role on the final microstructure and performance of the SOFC cells [9]. Regarding the differences between SOFC and SOEC modes, the higher steam content as well as the more difficult removal of hydrogen into the Ni-YSZ electrode in SOEC mode leads to

different microstructural requirements than SOFC mode [10]. As water molecules are more difficult to be transported due to their increased size in comparison with hydrogen molecules, the required porosity of Ni-YSZ for SOEC application is about 45%, while for SOFC mode it is about 35% [5,11].

In this respect, the authors have shown recently that using larger YSZ particles such as calcined YSZ instead of as-received YSZ during cell fabrication significantly enhances the cell electrochemical performance in SOEC mode where a high porosity is required to transfer the high steam content. However, the higher porosity of the cell as a result of using calcined YSZ leads to a decrease of the TPBs and the rate of electrochemical reactions in SOFC mode at the same time. The concentration polarization and activation polarization of the cell in this case seem to compensate each other and the fuel cell shows similar power performance to the cell which uses as-received YSZ in its anode [5].

Adding pore-formers such as flour, rice, corn starch, wheat, graphite, carbon black, and microspheres to increase the porosity of the nickel-YSZ anode support following reduction is a known technique to enhance gas diffusion since the nickel-YSZ cermet does not have sufficient porosity following reduction [10,12,13,14,15]. The presence of a high porosity as a result of the addition of a high pore-former content leads to improved gas diffusion but at the same time causes degradation of mechanical properties and a reduction of electronic and ionic conductivities since the contact points are reduced [16,17]. Liu et al. [10] used four different pore-formers such as polymethyl methacrylate (PMMA), potato starch, ammonium oxalate and ammonium carbonate in the Ni-YSZ electrode and realized that PMMA was the most promising pore-former for SOEC applications since it provided a high porosity and uniform pore size distribution in the microstructure. While large pores reduce the TPB length and as such the

power performance, very small pores can also obstruct the fuel gas and water vapor diffusion [18]. Therefore, it is important to understand the effect of pore-former content, shape and size on the Ni-YSZ anode microstructure which can affect the performance of the cell quite differently under SOFC and SOEC modes. This topic is the scope of the current research hoping to improve the underlying science behind the microstructure of SOECs.

Experimental Procedure

In this study, three different tubular fuel cells based on Ni-YSZ fuel electrodes were fabricated which were: *Graphite* cell: calcined YSZ + 30 vol.% graphite; *PMMA* cell: calcined YSZ + 30 vol.% PMMA; and *Mixture* cell: calcined YSZ + 15 vol.% graphite + 15 vol.% PMMA. The volume of the pore-formers added was 30% of the total volume of the NiO-YSZ in the anode. All Ni-YSZ anodes were fabricated by slip casting of a NiO-YSZ support followed by dip coating of a thin YSZ electrolyte and a thin porous YSZ layer as a scaffold for $Nd_2NiO_{4+\delta}$ (Nd-nickelate) infiltration. Nd and Ni salts were then infiltrated into the thin porous YSZ layer of the cells to form the cathode. In order to produce a suitable slip for casting the anode supported cells, as received YSZ powder (TZ-8Y, 8 mol% Y_2O_3, Tosoh) or its calcined form (calcined at 1500°C for 3 h), was mixed with 65 wt% NiO powder (Baker Chemicals) and water at a powder:water ratio of 1:1 at room temperature. The mixture was then milled at 120 rpm for 72 h in a plastic bottle with 5 mm zirconia balls. More water was added after milling to adjust the solid loading of the final suspension to 40%. The pH of the slip was set to 4.0 using 2% hydrochloric acid. In order to generate high porosity, the required quantity of pore-former (graphite (< 325 mesh, Sigma Aldrich) or PMMA (CA 6, Microbeads, Skedsmokorset, Norway)) was incorporated into the slip following pH adjustment, and then the suspension was mixed for 15 min prior to slip casting. To create the tubular support, the slip was cast into a plaster mold (previously prepared

from a tubular mandrel) and left for about 1 min, after which the excess slip was quickly poured out. The wet tube was then dried at room temperature for 1 h. The resulting drying shrinkage facilitates removal of the green tube. The green tube was further dried at 100°C in an oven, heated to 250°C (in case of PMMA) or 700°C (in case of graphite) for 1 h to eliminate the pore-former, and then pre-sintered under air at 1000°C for 3 h. Following each application of electrolyte or the thin porous YSZ layer for cathode application, the cell was sintered at 1350°C. No anode functional layer was coated on the Ni-YSZ support. The electrolyte and the thin porous YSZ layer formulas and dip coating procedure as well as Nd-nickelate (NNO) infiltration have been explained previously elsewhere [19,20,21,22]. Density and porosity (open and closed) measurements were carried out on slip cast and sintered pellets of each anode using Archimedes principle. The same pellets were used for calculation of the sintering shrinkage.

In order to measure the electrochemical performance of the cells, the open ends of the tubular cells were sealed to alumina tubes using a ceramic paste (Aremco Ceramabond 503). For the electrochemical experiments, platinum wire was coiled and tightly placed inside the tube to provide electrical contact. Gold wires were used for current collection at the oxygen electrode side, and gold paste (ElectroScience, ESL 8884-G) was used to improve current collection. Steam and hydrogen mixtures were introduced into the tubular cell through a smaller diameter alumina tube. Steam was supplied by the use of a direct vapour humidifier controlling the relative humidity (% RH) with a resolution of 1.3%. All gas lines located downstream of the humidifier were externally heated in order to prevent steam condensation. Electrochemical measurements were performed using a VSP Potentiostat/Galvanostat (Princeton Applied Research, Oak Ridge, USA). Current density-voltage (*j*-V) curves were collected in potentiodynamic mode from OCV (open circuit voltage) down to 0.5 V in SOFC mode, and from

OCV up to 1.5 V in SOEC mode, using a scan rate of 2.5 mA s^{-1}. Electrochemical impedance spectroscopy (EIS) measurements were performed using a sinusoidal amplitude signal of 20 mV in the frequency range of 100 kHz to 0.1 Hz.

Scanning electron microscopy (SEM) was carried out on the fuel cells using a Zeiss EVO LS15 EP-SEM instrument and a Carl Zeiss Merlin equipped with an Energy Dispersive Spectroscopy (EDS) INCA-350 system (Oxford Instruments, United Kingdom).

Results and Discussion

Microstructural Characterization

Figure 1a and 1b show the SEM images of the graphite and PMMA used to generate the porous Ni-YSZ anode. Graphite particles present a shape of flakes (ranging from about 5 to 10 µm) whereas PMMA particles are almost perfect spheres of about 6 µm in diameter. Figure 1c, d and e shows the microstructure of the Ni-YSZ anode (after NiO to Ni reduction) containing *graphite*, *mixture* and *PMMA* as the pore-former, respectively. Regardless of the pores generated by the pore-former, it can be observed that the *PMMA* cell has more sub-micron size pores which are formed during reduction of NiO to Ni. NiO-YSZ support porosity and shrinkage following sintering at 1350°C are shown in Table 1. As can be seen, the *graphite*, *PMMA* and *mixture* cells show about 51%, 41% and 45% open porosity, respectively. Despite using the same volume of pore-former in fabrication of the Ni-YSZ anode (30 vol.%), this result shows that the porous structure is affected by the sintering shrinkage. In the case of PMMA, the anode showed about 18% shrinkage and in the case of graphite it showed 15% shrinkage. This can be a reason for less porosity when PMMA was used as the pore-former.

The three types of studied cells were also observed under the SEM after the electrochemical measurements, as shown in Figure 2. Images (a), (b) and (c) show the microstructure of the

different layers of the three types of cells. Final dimensions of the cells are: ~450-550 µm Ni-YSZ support, ~10-15 µm YSZ electrolyte, ~20-25 µm NNO-YSZ oxygen electrode and ~10-15 µm NNO current collection layer. Images (d), (e) and (f) show the microstructure of the NNO-YSZ oxygen electrode. A homogeneous distribution of fine NNO grains (ranging from 50 to 100 nn) are observed in all cells. Finally, images (g), (h) and (i) shows the functional Ni-YSZ region next to the YSZ electrolyte. It is clearly observed that the *PMMA* cell exhibits finer porosity in the functional region which is considered to be the active area within the first 10 µm distance from the electrolyte where most of the electrochemical reactions occur. Ni and YSZ grains are both about 1 µm in size in these microstructures.

Electrochemical Characterization

The three different types of cells were characterized under both fuel cell and electrolysis modes using a fuel composition of 50%H_2O-50%H_2 inside the fuel electrode and static air at the oxygen electrode side. Electrochemical impedance spectroscopy (EIS) collected under OCV conditions is shown in Figure 3 (a) and the variation of the fitting resistances is also presented in Figure 3 (b). In these types of microtubular cells, usually up to four components are distinguished accounting for diffusion (oxygen gas phase and O^{2-} migration) and activation (charge transfer) at both electrodes [23,24,25]. In those cells, the contribution associated with diffusion at the oxygen electrode is almost negligible due to the small thickness of the oxygen electrode (~30-40 µm), especially in comparison with the fuel electrode supports (~500 µm). As a consequence, all EIS measurements were fitted using the equivalent circuit L-R_o-(R_1CPE$_1$)-(R_2CPE$_2$)-(R_3CPE$_3$), where L is an inductance, R_o the ohmic resistance, and (R_1CPE$_1$), (R_2CPE$_2$), (R_3CPE$_3$) are three resistance-constant phase elements.

The R_2 component, appearing at frequencies ranging from 2 to 5 kHz with capacitance values in the range of 10^{-4} Fcm^{-2}, is almost constant for the three types of studied cells. Experiments varying pO_2 (see supplementary material S1) confirmed that R_2 is the only variable component and, as a consequence, it was assigned to activation at the oxygen electrode. The R_3 component, appearing at frequencies ranging from 1 to 10 Hz with capacitance values in the range of 10 Fcm^{-2}, is also about constant for the three types of cells. This component is assigned to gas conversion at the fuel electrode, as it also decreases when increasing pH_2O (see supplementary material S2). This assignation is also consistent with other literature data [26,27]. This shows that, despite the different anode porosities, none of the cells present gas diffusion limitations. The main differences were found for the R_1 component (appearing at frequencies ranging from 15 to 20 kHz with capacitance values in the range of 10^{-5} Fcm^{-2}), typically attributed to activation at the fuel electrode, with the maximum resistance for the *graphite* cell and the minimum resistance for the *PMMA* cell. This is consistent with the observed microstructure shown in Figure 2, where the presence of PMMA pore former leads to an enhanced distribution of small pores, favouring charge transfer in the functional regions. In fact, the presence of pores formed by PMMA should facilitate the formation of finer pores compared with graphite in the functional regions of the studied cells. It is thought that PMMA pores affect hydrogen gas diffusion in the Ni-YSZ anode and as such the conversion of NiO to Ni in a manner such that finer pores form. The shrinkage of the support containing PMMA was also higher than the supports containing graphite or mixed pore-formers and this may also favour the formation of finer pores. The increased TPB length can increase the reaction rate and reduces the activation polarization. The use of mixtures of PMMA/graphite yields intermediate activation polarization as well as area specific resistance (ASR) values.

Typical *j*-V curves are plotted in Figure 4 and a summary of their electrochemical properties is shown in Table 2. The performance of the *graphite* cell is very similar to that reported by Hanifi *et al.* [5], fabricated with identical composition, indicating a good reproducibility of the fabrication process. As described in that work, the behaviour in electrolysis for this cell is better than in SOFC mode (see ASR values in Table 2). The optimized microstructure of the fuel electrode led to an increased performance in SOEC, especially at high current densities, as a consequence of easy gas diffusion through the pores of the support. On the contrary, slightly higher values are obtained in SOEC mode for both *mixture* and *PMMA* cells. In concordance with EIS experiments, the best electrochemical performance was found for the *PMMA* sample. For example, 818 and -713 $mAcm^{-2}$ were obtained in SOFC (at 0.5V and 800 ºC) and SOEC (at 1.3V and 800 ºC) modes, respectively.

In order to fully understand such observed differences between cells, EIS under current load was also performed (Figure 5 left). A summary of the fitting parameters is shown in Figure 5 (right). As previously explained, R_1 accounts for the activation at the fuel electrode, R_2 component to activation at the oxygen electrode and R_3 is assigned to steam/hydrogen gas phase diffusion at the fuel electrode. It is worth noting that, in general, the R_2 resistance decreases slightly in electrolysis mode possibly due to the excess oxygen stoichiometry of the Ruddlesden-Popper $Nd_2NiO_{4+\delta}$ phase favouring oxygen evolution, as previously reported by different authors [28,29,30]. On the other hand, the main differences were observed for the component assigned to activation at the fuel electrode, especially for the *graphite* cell, where R_1 increases in fuel cell mode and decreases in electrolysis mode. The reason for this phenomenon is still unclear and under investigation. The lower activation polarization of the cell containing PMMA can also be attributed to the finer pores formed in the functional region of the Ni-YSZ fuel electrode which

enhances the electrochemical reactions. In addition, all the cells show relatively similar R_3 values meaning that despite different porosity content and morphology coming from the different pore-formers, the fuel gas diffusion did not encounter problems and it may be unnecessary to have a highly porous fuel electrode. In any case, detailed experiments as a function of steam and hydrogen content are required to fully understand this effect.

Reversible Durability Studies

It was recently reported that electrolysis-induced degradation can be eliminated by reversibly cycling between electrolysis and fuel cell modes, similar to a rechargeable battery [31]. In fact, cycling studies on reversible SOFC/SOEC cells is under continuous investigation [32,33,34]. In the present study, we selected the *mixture* cell for cycling studies as it contains a mixture of both PMMA and graphite pore-formers. The selected conditions for the experiments were: 24 hours under a fixed voltage of 1150 mV (SOEC) followed by 24 hours under a fixed voltage of 700 mV (SOFC). This experiment was conducted for a total period of about 412 hours, as shown in Figure 6. Despite the initial fluctuations in electrolysis mode during the first 24 hours, the measured current density is approximately constant in both operation modes up to a period approaching 200 hours. From this point, it is then observed that during electrolysis mode there is always a slight degradation which seems to be recovered during the subsequent operation under fuel cell mode. As previously reported by Graves *et al.* [31], the typical microstructural degradation mechanism that occurs near the oxygen-electrode/electrolyte interface in SOEC mode [35,36,37] seems to be avoided.

Finally, in all the studied samples, there are no apparent signs of the typical SOEC degradation: neither agglomeration of nickel grains at the fuel electrode nor oxygen electrode delamination at

the electrolyte/electrode interface, as confirmed by SEM image analysis (see supplementary material S3 and Figure 2).

Conclusions

The results of the current study show that PMMA can be an ideal pore-former for generation of a microstructure performing well under both SOFC and SOEC operational modes. Despite an equal amount producing less porosity in the Ni-YSZ support when compared with graphite, the generated porosity (41%) appears to be sufficient for gas diffusion. Channels produced by PMMA also facilitate the formation of finer porosity next to the cell electrolyte which increases the rate of electrochemical reactions, reduces the activation polarization and as such enhances the power performance under both SOFC and SOEC modes. Durability studies under both fuel cell and electrolysis modes demonstrated that the cells are stable for a period of more than 400 hours.

Acknowledgements

The authors would like to acknowledge the Natural Sciences and Engineering Research Council of Canada (NSERC) for funding part of this research. The work was also funded by the Fundación Domingo Martínez, the Spanish Government (Ministerio de Economía y Competitividad) and the Feder Program of the European Union (MAT2015-68078-R project). LM acknowledges the internship agreement between CSIC and University of Bordeaux for the research stay at ICMA. The use of Servicio General de Apoyo a la Investigacion-SAI, Universidad de Zaragoza is finally acknowledged for the use of the electron microscopy facilities.

Table 1. Porosity and shrinkage of NiO-YSZ support following sintering at 1350°C.

Sample	Open porosity (%)	Closed porosity (%)	Shrinkage (%)
Graphite	51	4	15
Mixture	45	2	16
PMMA	41	1	18

Table 2. Summary of the electrochemical properties for the different studied cells.

Sample	Temp. (°C)	*j* at 0.5V ($mAcm^{-2}$)	*j* at 1.3V ($mAcm^{-2}$)	ASR_{SOFC} (Ωcm^2)	ASR_{SOEC} (Ωcm^2)
Graphite	600	293	-179	1.70	1.68
	650	363	-241	1.33	1.31
	700	429	-315	1.08	1.07
	750	556	-453	0.81	0.77
	800	653	-620	0.68	0.58
Mixture	600	293	-145	1.80	1.88
	650	376	-211	1.37	1.34
	700	495	-287	1.01	1.04
	750	548	-371	0.87	0.87
	800	619	-454	0.75	0.74
PMMA	600	441	-264	1.06	1.25

	650	560	-363	0.81	0.95
	700	677	-484	0.65	0.74
	750	757	-608	0.57	0.61
	800	818	-713	0.51	0.54

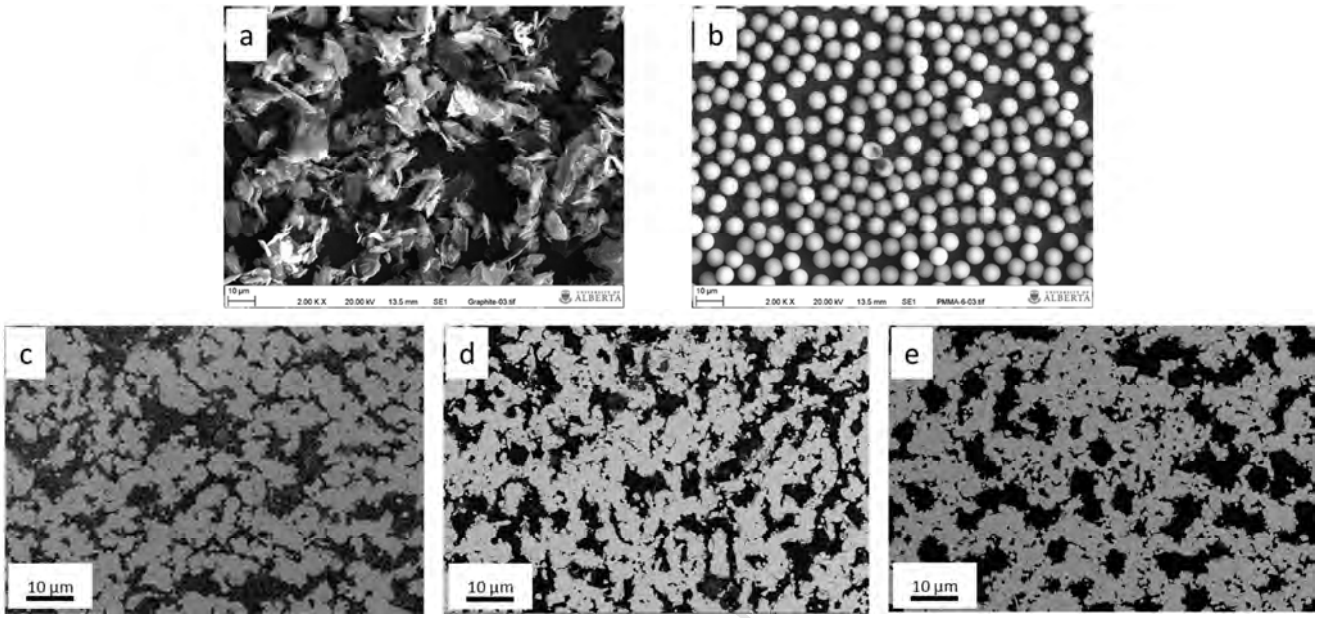

Figure 1. SEM images showing the typical morphology of the pore-formers used. (a): Graphite and (b): PMMA. SEM images showing the Ni-YSZ-pore distribution in the support for the *graphite* (c), *mixture* (d) and *PMMA* (e) cells.

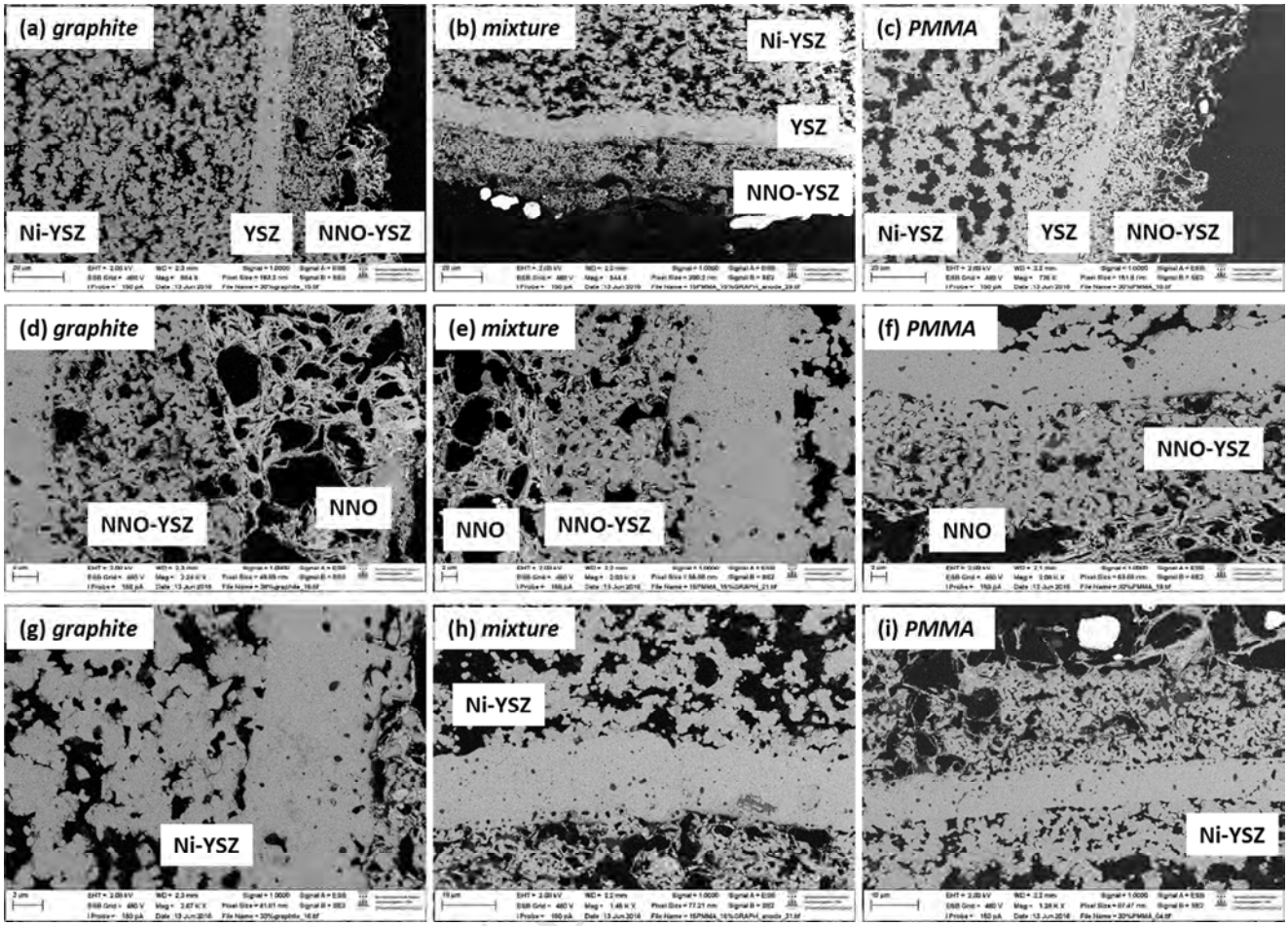

Figure 2. SEM images showing the microstructure of the three type of studied cells: (a), (b) and (c): general view showing fuel electrode (Ni-YSZ), electrolyte (YSZ), oxygen electrode (NNO-YSZ) and current collector (NNO); (d), (e) and (f): magnification showing the NNO-YSZ and NNO layers; (g), (h) and (i): magnification of the Ni-YSZ functional region.

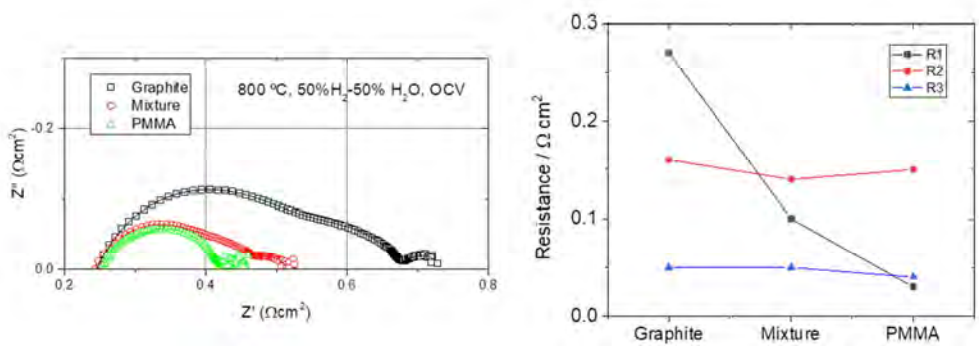

Figure 3. (a) Nyquist diagrams collected under OCV conditions at 800 °C just after NiO to Nireduction for the three types of cells; (b) Resistance fitting parameters from the Nyquist diagrams.

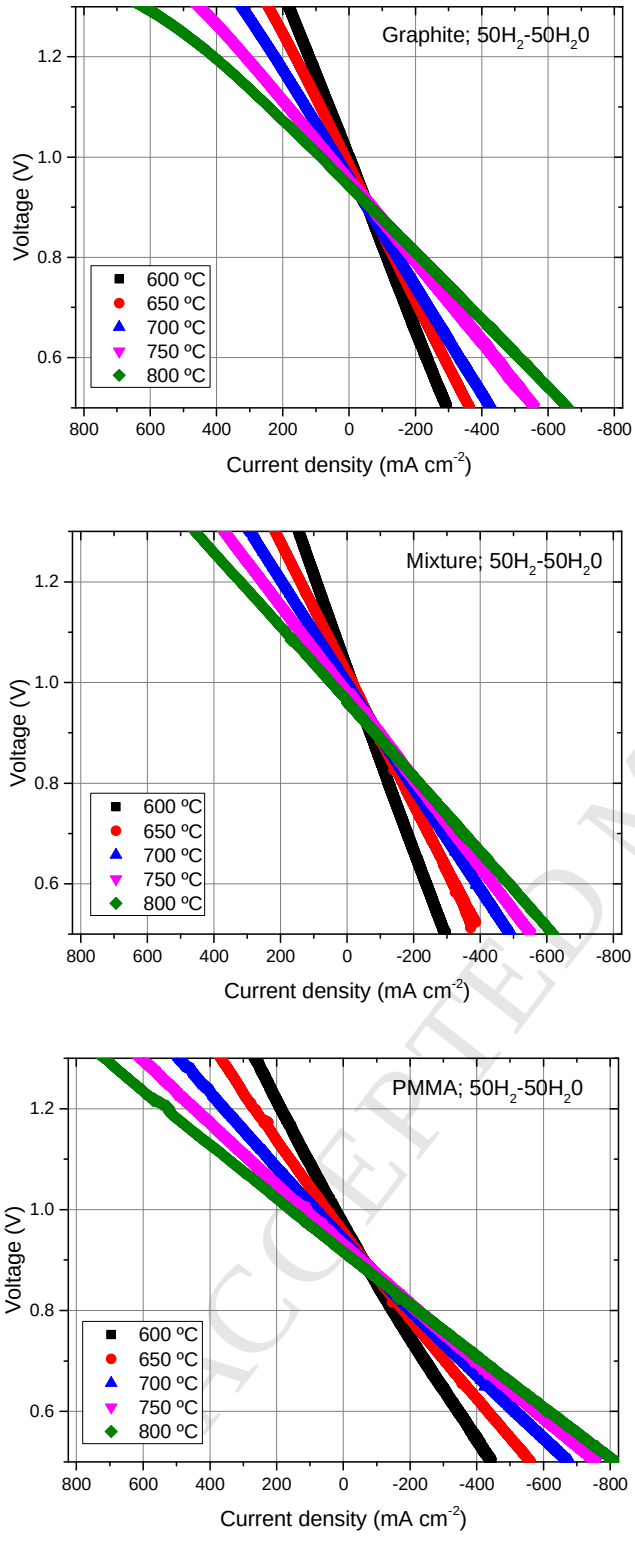

Figure 4. Current density (j) versus voltage (V) in both fuel cell and electrolysis modes at temperatures between 600 and 800 °C for the three types of cells.

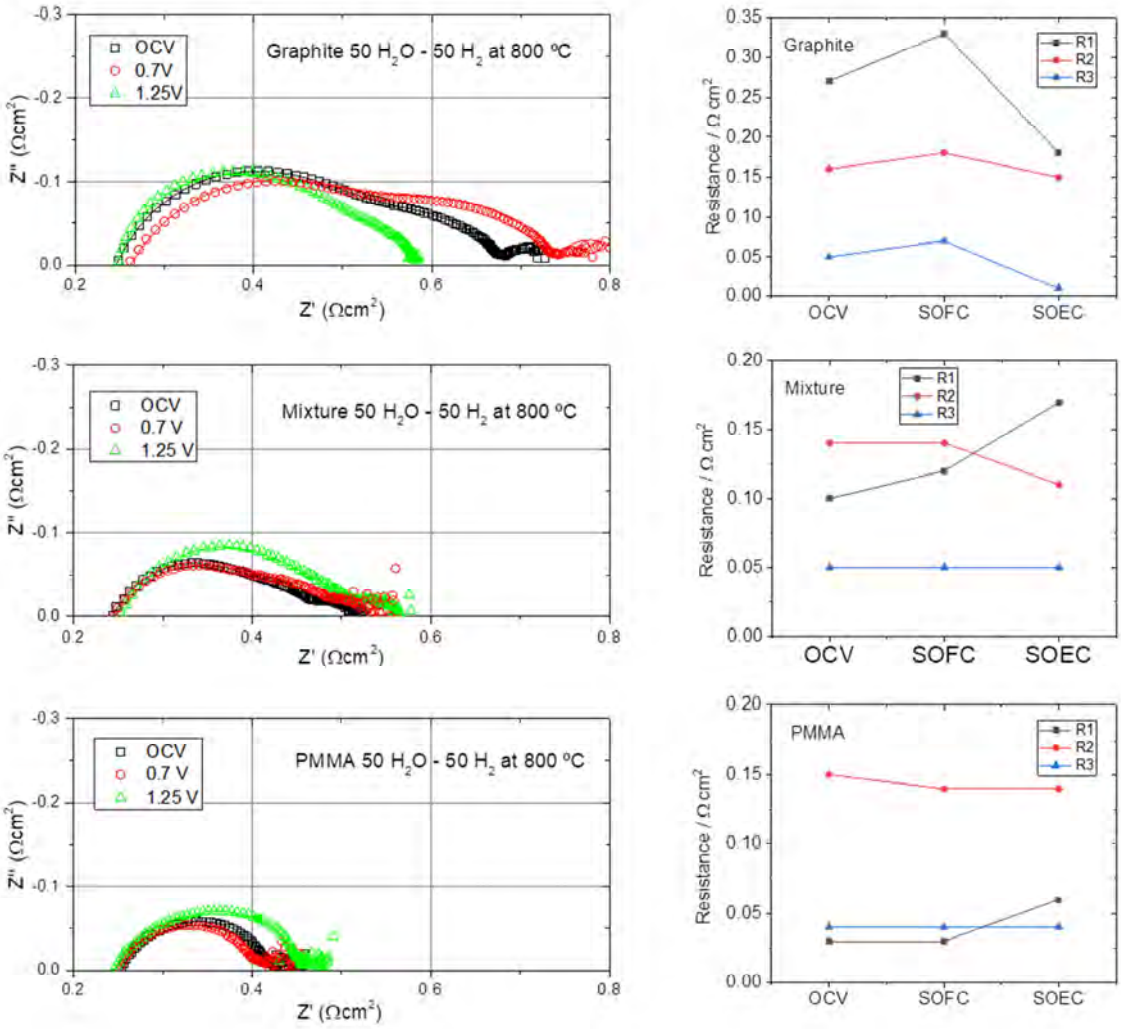

Figure 5. (left) Nyquist diagrams collected under OCV, 0.7 V (SOFC) and 1.25 V (SOEC) at 800 °C for the three types of cells; (right) Resistance fitting parameters from the Nyquist diagrams.

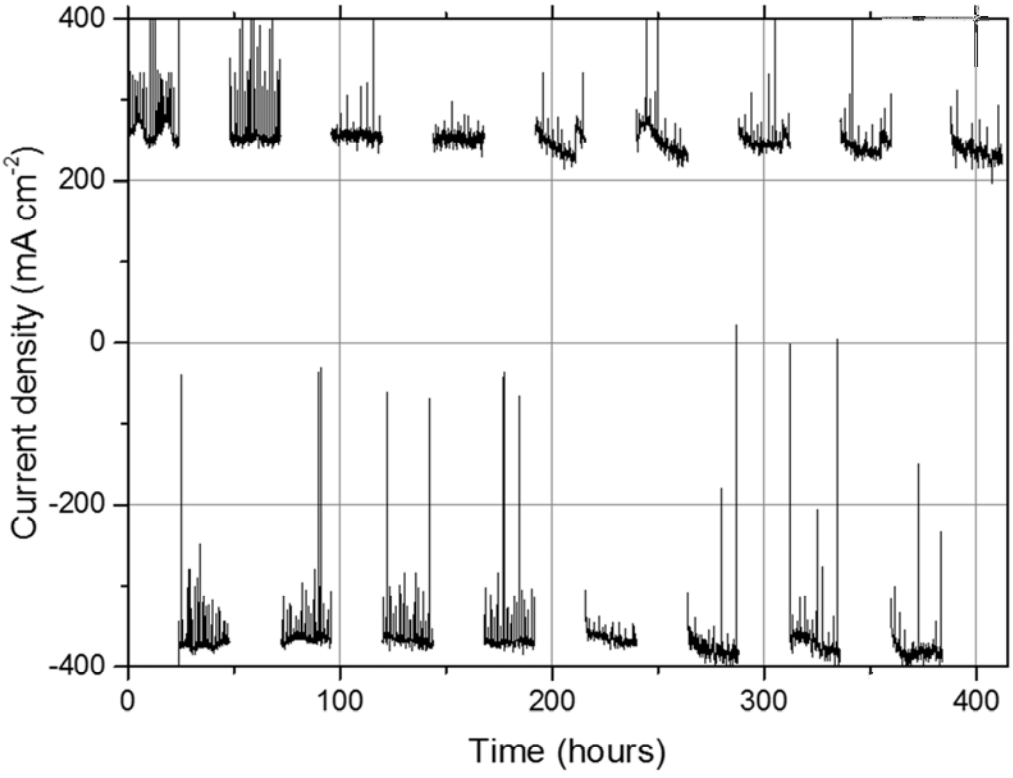

Figure 6. Reversible durability studies for the *mixture* cell by switching the voltage from 1150 mV (SOEC) to 700 mV (SOFC) every 24 hours, for a total period of about 412 hours.

References:

[1] M.A. Laguna-Bercero, Recent advances in high temperature electrolysis using solid oxide fuel cells: A review. J Power Sourc 2012;203:4-16.
[2] A.B. Stambouli, E. Traversa, Solid oxide fuel cells (SOFCs): a review of an environmentally clean and efficient source of energy. Renew Sustain Energy Rev 2002;6:433-455.
[3] S.D. Kim, H. Moon, S.H. Hyun, J. Moon, J. Kim, H.W. Lee, Performance and durability of Ni-coated YSZ anodes for intermediate temperature solid oxide fuel cells. Solid State Ion 2006;177:931-938.
[4] J.Y. Yoo, C.K. Cho, I.J. Shon, K.T. Lee, Preparation of porous Ni–YSZ cermet anodes for solid oxide fuel cells by high frequency induction heated sintering. Mater Lett 2011;65:2066-2069.
[5] A.R. Hanifi, M.A. Laguna-Bercero, N.K. Sandhu, T.H. Etsell, P. Sarkar, Tailoring the microstructure of a solid oxide fuel cell anode support by calcination and milling of YSZ. Sci Rep 2016;6:27359.
[6] A. Sanson, P. Pinasco, E. Roncari, Influence of pore formers on slurry composition and microstructure of tape cast supporting anodes for SOFCs. J Eur Ceram Soc 2008;28:1221-1226.
[7] K.R. Han, Y. Jeong, H. Lee, C.S. Kim, Fabrication of NiO/YSZ anode material for SOFC via mixed NiO precursors, Mater Lett, 2007;61:1242-1245.
[8] M. Mogensen, S. Skaarup, Kinetic and geometric aspects of solid oxide fuel cell electrodes. Solid State Ion 1996;86-8:1151-1160.
[9] H. Monzón, M.A. Laguna-Bercero, The influence of the reducing conditions on the final microstructure and performance of nickel-yttria stabilized zirconia cermets. Electrochim Acta 2016;221:41-47.
[10] M.Y. Liu, B. Yu, J.M. Xu, J. Chen, Influence of pore formers on physical properties and microstructures of supporting cathodes of solid oxide electrolysis cells. Int J Hydrogen Energy 2010;35:2670-2674.
[11] J.H. Lee, H. Moon, H.W. Lee, J. Kim, J.D. Kim, K.H. Yoon, Quantitative analysis of microstructure and its related electrical property of SOFC anode, Ni–YSZ cermet. Solid State Ion 2002;148:15-26.
[12] J. Kim, K.H. Cho, I. Kagomiya, K. Park, Structural studies of porous Ni/YSZ cermets fabricated by the solid-state reaction method. Ceram. Int. 2013;39:7467-7474.
[13] J.Y. Hu, Z. Lu, K.F. Chen, X.Q. Huang, N. Ai, X.B. Du, C.W. Fu, J.M. Wang, W.H. Su, Effect of composite pore-former on the fabrication and performance of anode-supported membranes for SOFCs. J Membr Sci 2008;318:445-451.
[14] H. Moon, S.D. Kim, S.H. Hyun, H.S. Kim, Development of IT-SOFC unit cells with anode-supported thin electrolytes via tape casting and co-firing. Int J Hydrogen Energy 2008;33:1758-1768.
[15] BI Arias-Serrano, ME Sotomayor, A Várez, B Levenfeld, H Monzón, MA Laguna-Bercero, A Larrea, High-performance Ni–YSZ thin-walled microtubes for anode-supported solid oxide fuel cells obtained by powder extrusion moulding. RSC Adv 2016;6:19007-19015.
[16] T. Talebi, M.H. Sarrafi, M. Haji, B. Raissi, A. Maghsoudipour, Investigation on microstructures of NiO–YSZ composite and Ni–YSZ cermet for SOFCs. Int J Hydrogen Energy 2010;35:9440-9447.
[17] B.A. Horri, C. Selomulya, H.T. Wang, Characteristics of Ni/YSZ ceramic anode prepared using carbon microspheres as a pore former. Int J Hydrogen Energy 2012;37:15311-15319.

[18] J.J. Haslam, A.Q. Pham, B.W. Chung, J.F. DiCarlo, R.S. Glass, Effects of the Use of Pore Formers on Performance of an Anode Supported Solid Oxide Fuel Cell. J Am Ceram Soc 2005;88:513-518.
[19] A.R. Hanifi, A. Torabi, X. Chen, S. Hill, P. Sarkar, T.H. Etsell, Development of Redox Resistant Fully Infiltrated Tubular SOFCs. J Electrochem Soc 2014;161:F391-F397.
[20] M.A. Laguna-Bercero, A.R. Hanifi, H. Monzon, J. Cunningham, T.H. Etsell, P. Sarkar, High performance of microtubular solid oxide fuel cells using Nd2NiO4+δ-based composite cathodes. J Mater Chem A 2014;2:9764-9770.
[21] A.R. Hanifi, M.A. Laguna-Bercero, T.H. Etsell, P. Sarkar, The effect of electrode infiltration on the performance of tubular solid oxide fuel cells under electrolysis and fuel cell modes. Int J Hydrogen Energy 2014;39:8002-8008.
[22] A.R. Hanifi, S. Paulson, A. Torabi, A. Shinbine, M.C. Tucker, V. Birss, T.H. Etsell, P. Sarkar, Slip-cast and hot-solution infiltrated porous yttria stabilized zirconia (YSZ) supported tubular fuel cells. J Power Sourc 2014;266:121-131.
[23] M.A. Laguna-Bercero, A.R. Hanifi, T.H. Etsell, P. Sarkar, V.M. Orera, Microtubular solid oxide fuel cells with lanthanum strontium manganite infiltrated cathodes. Int J Hydrogen Energy 2015;40:5469-5474.
[24] M.J. Lopez-Robledo, M.A. Laguna-Bercero, J. Silva, V.M. Orera, A. Larrea, Electrochemical performance of intermediate temperature micro-tubular solid oxide fuel cells using porous ceria barrier layers. Ceram Int 2015;41;7651-7660.
[25] H. Monzón, M.A. Laguna-Bercero, Highly stable microtubular cells for portable solid oxide fuel cell applications. Electrochim Acta 2016;222:1622-1627.
[26] S. Primdahl, M. Mogensen, Gas Conversion Impedance: A Test Geometry Effect in Characterization of Solid Oxide Fuel Cell Anodes. J. Electrochem. Soc. 1998; 145:2431-2438.
[27] A. Bertei, G. Arcolini, J.P. Ouweltjes, Z. Wuillemin, P. Piccardo, C. Nicolella, Physically-based deconvolution of impedance spectra: interpretation, fitting and validation of a numerical model for lanthanum strontium cobalt ferrite-based solid oxide fuel cells. Electrochim. Acta;208:129-141.
[28] MA Laguna-Bercero, H Monzón, A Larrea, VM Orera, Improved stability of reversible solid oxide cells with a nickelate-based oxygen electrode. J Mater Chem A 2016;4:1446-1453.
[29] F. Chauveau, J. Mougin, J. M. Bassat, F. Mauvy and J. C. Grenier, A new anode material for solid oxide electrolyser: The neodymium nickelate Nd2NiO4+δ. J Power Sourc 2010;195:744-749.
[30] MA Laguna-Bercero, N Kinadjan, R Sayers, H El Shinawi, C Greaves, SJ Skinner, Performance of La2–xSrxCo0. 5Ni0. 5O4±δ as an Oxygen Electrode for Solid Oxide Reversible Cells. Fuel Cells 2011;11:102-107
[31] C. Graves, S. D. Ebbesen, S. H. Jensen, S. B. Simonsen, M. B. Mogensen, Eliminating degradation in solid oxide electrochemical cells by reversible operation. Nature Mater 2015;14: 239–244.
[32] J. Myung, D. Neagu, D.N. Miller, J.T.S. Irvine. Switching on electrocatalytic activity in solid oxide cells. Nature 2016;537:528–531.
[33] K. Chen, S. S. Liu, N. Ai, M. Koyama, S. P. Jiang, Why solid oxide cells can be reversibly operated in solid oxide electrolysis cell and fuel cell modes? Phys Chem Chem Phys 2015;17:31308-31315.

[34] L. Zhu, B. Wei, Z. Wang, K. Chen, H. Zhang, Y. Zhang, X. Huang, Zhe Lü, Electrochemically Driven Deactivation and Recovery in PrBaCo2O5+δ Oxygen Electrodes for Reversible Solid Oxide Fuel Cells. Chem Sus Chem 2016;9:2443–2450.

[35] MA Laguna-Bercero, R Campana, A Larrea, JA Kilner, VM Orera, Electrolyte degradation in anode supported microtubular yttria stabilized zirconia-based solid oxide steam electrolysis cells at high voltages of operation. J Power Sourc 2011;196:8942-8947.

[36] A.V. Virkar, Mechanism of oxygen electrode delamination in solid oxide electrolyzer cells. Int. J. Hydrogen Energy 2010;35:9527–9533.

[37] MA Laguna-Bercero, VM Orera, Micro-spectroscopic study of the degradation of scandia and ceria stabilized zirconia electrolytes in solid oxide electrolysis cells. Int J Hydrogen Energy 2011;36:13051-13058.